Testbed for Radio Astronomy Interference Characterization and Spectrum Sharing Research

Stefan Tschimben
Dept. of Computer Science
University of Colorado Boulder
Boulder, CO, USA
stefan.tschimben@colorado.edu

Arvind Aradhya
Dept. of ECEE
University of Colorado Boulder
Boulder, CO, USA
arvind.aradhya@colorado.edu

Georgiana Weihe
Dept. of Computer Science
University of Colorado Boulder
Boulder, CO, USA
georgiana.weihe@colorado.edu

Mark Lofquist
Dept. of Computer Science
University of Colorado Boulder
Boulder, CO, USA
mark.lofquist@colorado.edu

Alexander Pollak
Science & Engineering Operations
SETI Institute
Mountain View, CA, USA
apollak@seti.org

Wael Farah
Science & Engineering Operations SETI Institute
Mountain View, CA, USA
wfarah@seti.org

David DeBoer
Radio Astronomy Lab
University of California Berkeley
Berkeley, CA, USA
david.deboer@berkeley.edu

Kevin Gifford
Dept. of Computer Science
University of Colorado Boulder
Boulder, CO, USA
kevin.gifford@colorado.edu

2023 IEEE Aerospace Conference | 978-1-6654-9032-0/23/$31.00 ©2023 IEEE | DOI: 10.1109/AERO55745.2023.10115653

***Abstract*—As radio spectrum becomes increasingly scarce, co-existence and bidirectional sharing between active and passive systems becomes a crucial target. In the past, spectrum regulations conferred radio astronomy a status on par with active services, thereby protecting their extreme sensitivity against any harmful interference. However, passive systems are likely to lose exclusive allocations as capacity constraints for active systems increase. The resulting increase in ambient radio frequency noise from various terrestrial and non-terrestrial emitters can only be mitigated with informed collaboration between active and passive users. While coexistence using time-division spectrum access has been proposed in the past, a more dynamic approach following the CBRS sharing principle promises greater spectral occupancy and efficiency, enabled by a spectrum access system capable of constantly monitoring the ambient RF environment. Instead of simply minimizing the potential for any "harmful" interference to passive users, the goal is to use good engineering to enable sharing between active and passive users. To this end, this research created a Software Defined Radio (SDR)-based testbed at the the Hat Creek Radio Observatory to quantitatively characterize the radio-frequency environment, and flag potential sources of radio frequency interference in the vicinity of the Allen Telescope Array. Sensor validation was carried out via data analysis of I/Q data collected in well-characterized RF bands. Results so far from ground and drone-based surveys are consistent with the expected sources of interference, based on both the deployment of static RF transmitters in the Hat Creek/Redding area as well as the interference detected in telescope observations themselves.**

***Index Terms*—Radio Astronomy, Interference, Cognitive Radio, SDR, Noise, Instrumentation**

This work was supported by the National Science Foundation under Grant 2030233 and Grant 2139964.

978-1-6654-9032-0/23/$31.00 ©2023 IEEE

I. Introduction

Frequent travelers or moviegoers know the moment when you're asked to put your mobile phone into airplane or silent mode to keep it from interfering with the movie experience or the flight. While these devices actively accessing the radio spectrum are easier to address, passive users face additional challenges in an environment were access to the limited radio spectrum keeps increasing in value. As an increasing number of government and industry services is asked to share the spectrum, radio astronomy will eventually have to face the potential of sharing between active and passive users. Still only a concept in the regulatory domain, research in bi-directional sharing sharing between radio astronomy and active services has the potential to not only address future spectrum scarcity challenges but furthermore provide a path forward for other passive service that will face the need to share radio spectrum with active services.

Sharing spectrum raises a number of concerns for radio astronomy. While optical astronomy is hampered by light pollution, radio astronomy is much more concerned about radio frequency interference (RFI) [1]. Since signals from astronomical observations are extremely weak and easily drowned out by human made transmissions, making astrophysical observations becomes increasingly more difficult if the observed frequency band is shared with active users in time or frequency [1], [2]. Most radio telescopes in fact can be considered about 150 dB more sensitive than a cellular receiver, making radio telescopes highly susceptible to man-

made RFI [3].

Still, as the Passive and Active Spectrum Sharing (PASS) working group highlighted, spectrum sharing between passive and active systems will be crucial for future radio spectrum access [4]. To further improve efficient spectrum use and to investigate the challenges of creating a dynamic radio spectrum environment for radio astronomy, this research sets out to create a RFI testbed at the Hat Creek Radio Observatory (HCRO) located in northeastern California. This testbed is used to assess the spectral environment at HCRO, to determine and measure sources of RFI, and ultimately to create a national radio dynamic zone (NRDZ) by extending a spectrum access system (SAS) to coordinate radio astronomy with active users.

II. Background

It took more than 20 years from the first radio astronomical observation to recognize radio astronomy as an important use of the radio spectrum and to protect its observations on a regulatory basis from interference across multiple frequency bands [5]. Radio astronomy was not recognized as a ”radio service” until the World Administrative Radio Conference (WARC) of 1959, where the first dedicated band from 1400 to 1427 MHz was allocated to radio astronomy, granting radio astronomy protection from interference on the hydrogen line [6], [7]. Over the next 20 years, recognition for radio astronomy’s contribution to major technical advances continued to grow and additional spectrum allocations were finally made in 1963, 1971, and 1979. These national spectrum allocations did not only provide radio astronomy services with access to further molecular spectral lines, but additionally aimed for the first time at promoting international coordination for radio astronomy protection. To this day, radio astronomical observations have resulted in the discovery of more than 550 spectral lines across the frequency range from 0.8 to 350 GHz, exoplanets, fast radio bursts, and the discovery of the cosmic microwave background [8], [9].

Internationally, the passive use of the electromagnetic spectrum is regulated by the Radiocommunication Sector of the International Telecommunications Union (ITU-R) with binding outcomes negotiated every three to five years by the World Radiocommunication Conference (WRC). These outcomes are then matched on a national level by domestic regulations, e.g. by the Federal Communications Commission (FCC) for non-federal and by the National Telecommunications and Information Administration (NTIA) for federal use within the United States [7]. While regulations attempt to give radio astronomers protection from interference in the most essential frequency bands, regulations struggle to protect radio astronomy from interference from adjacent channels and unintentional emitters. As a result, the vast majority of radio astronomy sites has historically been placed in remote locations or valleys in order to minimize interference from man-made sources or on higher elevations to avoid as much water vapor as possible when observing higher frequency bands while also using traditional RFI mitigation methods, including RF filters, post-processing of data, discarding corrupted data samples, and local RFI mitigation [7], [10], [11]. Most observatories can be found inside a Radio Quiet Zone (RQZ), which usually consists of an exclusion zone limiting the use of the radio spectrum and a coordination zone with limited transmit power requirements, in order to further increase protection from a variety of sources of interference [12]. One example can be found at the National Radio Astronomy Observatory (NRAO) in Green Bank, WV, where RFI suppression is achieved with the help of a National Radio Quiet Zone (NRQZ) established in 1958 by the FCC [13]. However, while the ITU emphasizes in its recommendation RA.769 (ITU-R RA.769) that radio astronomy services have been responsible for some of the most fundamental astronomical and major technical advances in the past five decades [14], [15] emphasizes that NRQZs are neither globally adopted, nor enough to protect radio astronomy sites from interference caused by satellite networks in many locations, nor sustainable as urbanization increases, making new protection mechanisms necessary.

To ensure radio astronomy can continue operating in an environment that allows for major technological advances it is crucial to protect the service from interference. Interference for radio astronomy is defined in ITU-R RA.769 as the ”unwanted but detectable portion of a desired observation that has the potential to either degrade or inhibit the successful conduct of the observation” [14]. ITU-R RA.769 further describes harmful interference for radio astronomy as interference that causes a change in amplitude equal to 10% of the RMS noise or increases the uncertainty of the measurements by 10%. However, interference from terrestrial transmissions is no longer the only concern. Transmissions from aircrafts, spacecrafts, satellites, and the moon are increasingly becoming a concern for radio astronomy. ITU-R RA.1513 for instance dictates that harmful interference from a satellite network should affect less than 2% and from all systems less than 5% of the aggregate data [16].

As the sensitivity of radio telescopes increases in order to achieve better results, transmissions from a variety of sources, inside and outside of the observed band, are increasingly being captured through the telescopes side lobes [1], [2], [12], [17]. Even though regulations by the Federal Communications Commission (FCC) and agreements by the International Telecommunications Union (ITU) can be effective at preventing some interference, research has shown that even transmitters at distances beyond 100 km can be problematic [3]. Additionally, signals from low-earth-orbit (LEO) satellites leaking into protected radio astronomy bands can be an issue even in remote locations [1]. Sharing spectrum with radio astronomy would not only have to consider a much larger protection area, but furthermore be adaptive enough to react to terrestrial and satellite signals. A number of additional challenges need to be considered when sharing spectrum with radio astronomy and scheduling telescope observations, including logistical and environmental factors such as weather and ionospheric perturbations [11]. While scheduling observations dynamically in accordance with expected interference has been considered [18], considering all possible factor in dynamic observation

windows can become highly complex.

Historically, many mechanisms have been put in place to protect radio astronomy from interference, but as the spread of devices accessing the radio spectrum increases - 13.1 billion wireless connected devices by 2023 [19] -, previous protection mechanisms are proving insufficient and potentially unsustainable. While systems such as the Citizen Broadband Radio Service (CBRS) include provisions for protection zones, exclusive access to the radio spectrum and restrictive protection zones in the future might have to face a more dynamic mode of sharing as the demand for radio spectrum access by consumer devices continues to grow. As exclusive spectrum access is increasingly replaced by complex sharing arrangements, designing spectrum sharing models suited for sharing between radio astronomy and various active services will be vital to avoid harmful interference [20]. In fact, while spectrum sharing can result in more efficient spectrum use, it also has the potential to negatively impact passive users such as radiometry and radio astronomy. According to [21], coexistence with radio astronomy services at 1 GHz with a transmit power as low as 1 nW would require maintaining a safe distance of 1050 km from the passive service to avoid violating ITU-R Recommendation RA.769-2. Still, a system such as the Spectrum Access System used for the Citizen Broadband Radio Spectrum has considerable potential to solve the wide ranging coordination issues and avoid unnecessary interference. Additionally, [20] assumes free-space path loss, which, given the general location of observatories, is not guaranteed and often blocked by obstacles.

A system such as CBRS, where radio astronomy could be considered a primary user during radio astronomical observations, could alleviate many coordination and scheduling issues by allowing the radio astronomy facility to be in command of when protection is needed and let the frequencies be used freely otherwise. A crucial component of any spectrum sharing system is the ability to sense the spectrum for transmissions in order to prevent and identify potential sources of RFI, which can have a multitude of negative effects on radio astronomical observations: from misleading to corrupted observations and even the loss of data and hardware impairments [11]. The importance of addressing RFI is further emphasized by Bolli et al. highlighting the value of continuous RFI monitoring for optimal radio astronomy operations by demonstrating the capabilities of continuous RFI monitoring in the form of a mobile monitoring station [18]. The mobile station, deployed in Italy in multiple locations around the Sardinia Radio Telescope (SRT), used an Agilent PSA E4446A spectrum analyzer inside the mobile RFI monitoring station with antennas covering frequencies from 0.29 GHz to 24 GHz to not only identify RFI but also determine that the detected interference was not coming from the expected nearby source, but instead from malfunctioning equipment 60 km away [18]. A similar mobile station was deployed effectively around the Medicina radio-astronomical observatory near Bologna, Italy [18].

In addition to monitoring at the SRT, radio astronomy research increasingly recognizes the importance of continuous RFI monitoring. Some recent examples include measuring horizontal RFI with a copper discone antenna in Malaysia covering up to 2.8 GHz for 24 hours [22]; investigating RFI using handheld spectrum analyzers around the MeerKat telescope in South Africa, where L-band frequencies are corrupted by RFI from GSM DME, and GPS sources, concluding that anything from solar panels, to electric fences, diesel generators, 5.8 GHz wireless links, GMS, DME, and GPS sources contribute to RFI [2], [23]; measuring RFI in Indonesia using two spectrum analyzers and the Square Kilometre Array (SKA) protocol [24]; and surveying the RFI environment for a new radio astronomy observatory in Turkey covering frequencies from 1 GHz to 40 GHz [25].

While radio telescopes rarely point at terrestrial sources of interference directly, non-terrestrial sources such as satellite communication remain an issue. As a result, the goal of this testbed is to create a prototype for a national radio dynamic zone (NRDZ) at the Hat Creek Radio Observatory (HCRO) by deploying stationary sensors for continuous RFI monitoring in multiple locations to determine sources of interference and by establishing a coordination system similar to CBRS where radio telescopes and satellite communication can coexist. While a somewhat similar approach was researched in [26], instead of sharing spectrum between the Giant Metrewave Radio Telescope and satellite communication the goal of [26] was to co-exist with satellite interference and digitally remove known satellite interference. This testbed instead seeks to determine satellite free observation windows and create an automated system that allows radio astronomy to schedule observations without interference while also opening up the area for spectrum sharing during observation-free windows.

In a first step of establishing the testbed, 5 low-cost sensors have been deployed around HCRO that continuously sweep the frequencies from 400 to 1800 MHz (see Figure 1). To verify the efficiency of HCRO's remote location at protecting it from RFI, a drone was flown in 3 different locations at 4 different heights with an additional sensor attached to evaluate the RFI environment at elevated positions. The results of these drone surveys are compared with the results of the 5 stationary ground sensors. Table I lists the 5 main sensors located on the HCRO site with their exact location and height above ground, as well as the locations of the drone surveys and their distance to a known transmitter. The next section is organized as follows: section III will begin with a description of the sensor hardware, followed by a brief description of the data collection software used to execute the RF surveys, and conclude with a description of the drone survey parameters.

III. The Testbed

A. Hardware

As described in Section II, current implementations of dedicated RFI monitoring equipment at various radio astronomy facilities are based on the use of spectrum analyzers. The cost of this approach does not lend itself to the deployment of multiple sensors and is subject to several drawbacks as a single or small number of sensors severely constrains the spatial

Fig. 1: **Sensor Locations**

TABLE I: **Ground Stationary Testbed**

	Sensor Location		Sensor Antenna	
ID	*Name*	*Lat./Long.*	*H.A.G.*	*Dist. to Tx*
S1	Main Office	40.8172N 121.4690W	27.5ft	88ft
S2	Gate	40.8257N 121.4701W	13ft	3,187ft
S3	CHIME	40.8165N 121.4640W	13.2ft	1,468ft
S4	West-740	40.8167N 121.4720W	13.4ft	766ft
S5	North-1740	40.8215N 121.4682W	10.7ft	1,667ft

diversity of RF sampling. Assuming a uniform distribution, a single spectrum analyzer provides at best an averaged estimate of the background RFI and in the worst case a noise estimate that is below the RFI incident on the radio telescope if the sensor is in a more favorable location than the telescope. While spectrum analyzers have been the only available instruments for RFI monitoring until recently, their high cost and not leveraged capabilities when used as dedicated RFI monitors make the use of spectrum analyzers less ideal. Additionally, such a system is usually constrained to operate in a single, contiguous slice of the frequency spectrum of interest and therefore is not suited to track frequency-variant transient signals. Given that RFI monitoring or developing custom RFI monitoring systems is outside the scope of radio astronomy services, a commercial, off-the-shelf (COTS) solution in the form of software defined radios (SDR) is instead employed for this testbed research.

While neither spectrum analyzers, nor SDRs approach the sensitivity limits of radio telescope receivers, SDRs offer an advantageous trade-off between sensitivity and cost. Even spectrum analyzer based RFI monitors require dedicated RF components to detect signals at levels close to the sensitivity of radio telescopes. Consequently, to keep cost low while achieving results on a level similar to a spectrum analyzer, a range of connected RF components is used to design of a dedicated RFI monitoring system based on an SDR. The testbed designed and installed via this work investigates the feasibility of the aforementioned approach.

The primary hardware requirements of the sensor node design are as follows: 1) be sensitive to terrestrial and non-terrestrial RFI at the levels expected in the vicinity of the Allen Telescope Array; 2) operate across a majority of the frequency bandwidth of operation of the ATA; 3) minimize unintentional emissions from the sensor itself. A block diagram of a single stationary SDR based sensor is depicted in Figure 2. Each sensor is comprised of three primary parts: an omnidirectional antenna, a pre-amplifier, and an electro-magnetic interference (EMI) enclosure.

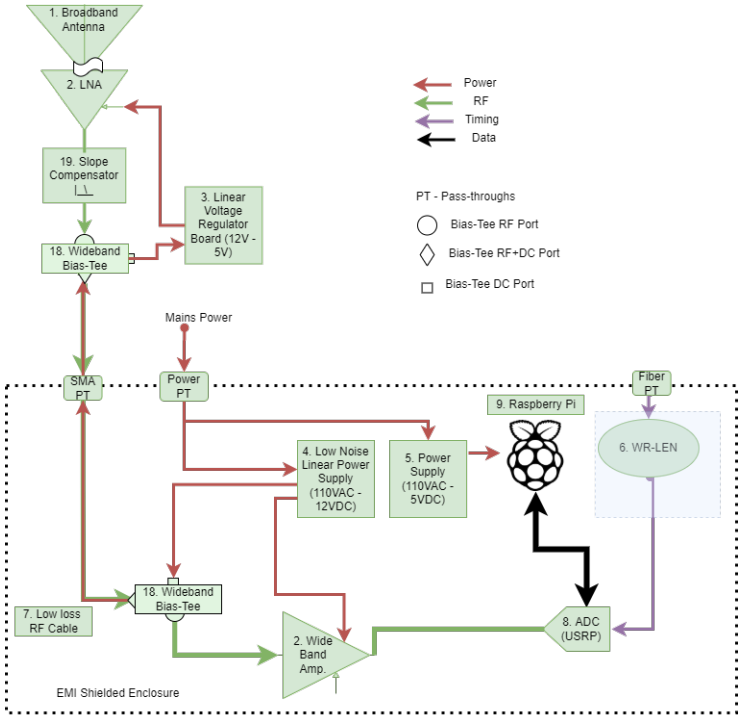

Fig. 2: **Block Diagram of Sensor Node**

An omnidirectional antenna not only has the advantage of ensuring the node's sensitivity to RFI from as many directions as possible, but furthermore preserves the ability to perform rogue source localisation by simply deploying multiple sensor nodes. By using multiple nodes, an interferers location can be determined using magnitude, phase, or time of arrival information, for instance. To minimize negative effects of RF propagation behavior, the nodes are designed to perform phase synchronized sampling. The Keysight N6850A antenna is favored for this testbed due to its mostly frequency independent

uniform radiation pattern with a VSWR of less than 2.5 from 450 MHz to 6 GHz and an average gain of -1 dBi (see Figure 3). The antenna's effective wide-bandwidth operation makes it ideal for multiple configurations targeting different frequency bands.

Unfortunately, due to availability issues only two Keysight antennas could be obtained at this time. These are installed at locations 2 and 3 (see Table I). For the remaining locations, the Aaronia OmniLog 30800 antenna has been selected as a viable alternative. While not possessing as much gain or uniformity as the N6850A with a VSWR of less than 3 from 700 MHz to 8 GHz and an average gain of ∼ -5 dBi, the Omnilog antenna is far less expensive and, most importantly, in stock. Both the N6850A and the OmniLog 30800 are linearly polarized and mounted vertically.

The antenna is followed by the pre-amplifier, which is comprised of a low-noise amplifier (LNA), a bias-tee, and a low drop-out linear voltage regulator circuit board. These components are housed in a 4" weather-proof junction cube. The antenna is mounted on top of the pre-amplifier box to minimize signal path length and thereby attenuation between the antenna and the LNA. The pre-amplifier amplifies the signal as quickly as possible, prior to the addition of losses due to attenuation and noise. Using a pre-amplifier can further reduce the negative effects of using an omnidirectional antenna, such as a reduced gain potential. The noise figure of the entire system, and therefore the sensitivity, is largely determined by the noise-figure of the first stage. As a result, the choice of LNA has a large impact on the overall system temperature. Because of the trade-off between the noise-figure and the gain of the LNA, the overall system gain is split between two amplifiers, where a low-noise figure amplifier is prioritized for the first stage.

Additionally, two different LNAs are used to monitor different regions of the target spectrum. For the frequency range from 400 to 1800 MHz a MiniCircuits ZKL-33ULN-S+ is chosen, providing a noise figure of less than 0.5 dB and available gain from 47 to 24 dB. For 1.8 to 6 GHz a MiniCircuits ZX60-63 GLN+ is selected with noise figures of less than 1.5 dB and a gain of 31.5 dB to 24 dB. Since the gain varies significantly over both LNA's operational frequency range, flattening the response across the passband is achieved by incorporating a slope-compensator with a similarly frequency dependent attenuation. For ease of assembly, this attenuator is placed outside the pre-amplifier box inside the EMI enclosure. The output of the pre-amplifier is then connected via an RF cable to the input of the EMI enclosure.

The final piece of the sensor node is the EMI enclosure, a modified Ramsey Test Solutions STE2300M EMI enclosure. The Ramsey STE2300 shielded enclosure has exterior measurements of 6.2" x 0.0" x 12.0" and interior measurements of 5.2" x 8.0" x 11.0" and weights approximately 10 lbs. All previous components have been analog without independent signal sources. However, the SDR and the computing host interfacing with the SDR are digital components. These are necessarily driven by clock signals, which can have transients

Fig. 3: **Installed Sensor Node showing the Keysight N6850A Antenna, the pre-amplifier box and the EMI enclosure inside the open field cabinet**

and the SDRs local oscillator can be a source of EMI. As a result, in order to minimize unintentional emissions from sensor components as well as external interference, these components are housed inside the same EMI enclosure. Minimizing unintentional emissions is especially important due to the sensors' close proximity to the ATA dishes and the interference such leakage could cause to the highly sensitive amplifiers in the telescopes.

The STE2300M EMI box has conductive gaskets lining the opening, which forms a tight, compressive seal when the box is closed. This leaves pass-through connections for power as the primary route through which EMI may leave and enter the box. To minimize this risk, the pass-through is appropriately filtered. Additionally, while the inside of the original EMI box came covered with RF-absorbers, it was revealed during operation that this led to poor thermal conductivity between the active components in the enclosure. Operational temperatures inside the box reached about $70^{\circ}C$ during periods when the ambient external temperature was about $35^{\circ}C$. As a result, this RF-absorber was removed from all sides, except for the top lid to keep leaked EMI to a minimum.

The inside of the EMI enclosure is divided into a two parts, as demonstrated in Figures 4 and 5. The lower half contains a switched mode power supply (MeanWell LRS-35-5), which provides DC voltage to the Raspberry Pi host and the White-Rabbit LEN (WR-LEN), and a linear power supply

(Bel Power Solutions HB12-1.7-AG) to provide DC voltage to the analog components. The WR-LEN terminal node provides both a timing reference signal in the form of a 10 MHz sinusoidal clock signal as well as network connectivity via a CAT-6e cable to the Raspberry Pi. The input to the WR- LEN is a single-mode optical fibre cable via an SFP connector, through which it receives a copy of the temperature controlled oscillator HCRO station clock. This clock signal is used for synchronized sampling across the ATA. Complete separation between the analog and digital components is usually pursued to avoid cross-talk between ground-planes. The power supplies are in immediate electrical and thermal contact with a metallic mounting plate, which in turn is in contact with the bottom of the box. The bottom of the box is connected to the local earth potential via the power cable. To provide fault protection, this section also contains AC mains fuses.

The Ethernet, power, and clock sources are connected through the mounting plate of the top-section. This top section comprises all the remaining analog components, as well as the Raspberry Pi and the Ettus Research B200-mini-i SDR. The analog components are comprised of the slope compensator (Minicircuits VEQY-6-63+), a wide-band gain-block (Mini-circuits ZX60-14012L-S+), and the same bias-tee used in the pre-amplifier (Minicircuits ZX85-12G-S+). The RF signals are connected by high-quality, twisted pair, low-loss RF cables from AtlantecRF.

The resulting system noise temperature at three frequencies is: 557 K at 400 MHz, 186 K at 1800 MHz, and 330 K at 5000 MHz.

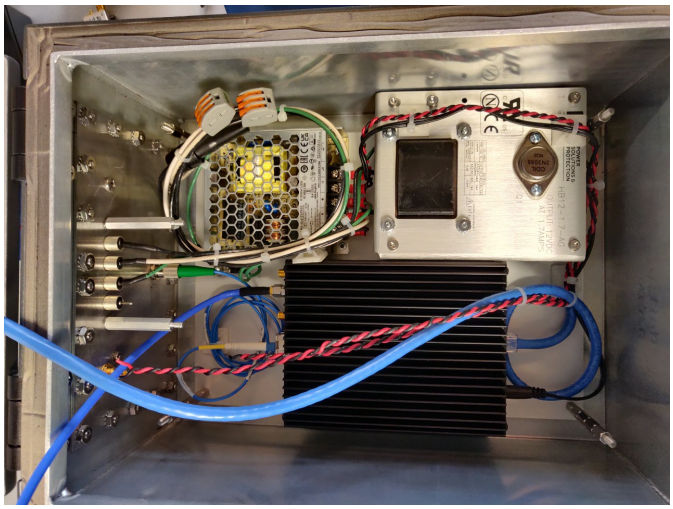

Fig. 4: **Bottom level of the EMI Enclosure**

[htbp]

B. Software

The main software components used for the testbed surveys are located on the Raspberry Pi 4 Model-b single board computers (SBC). Each SBC is equipped with a 64 GB SanDisk Ultra MicroSD card hosting a 32-bit version of Raspberry

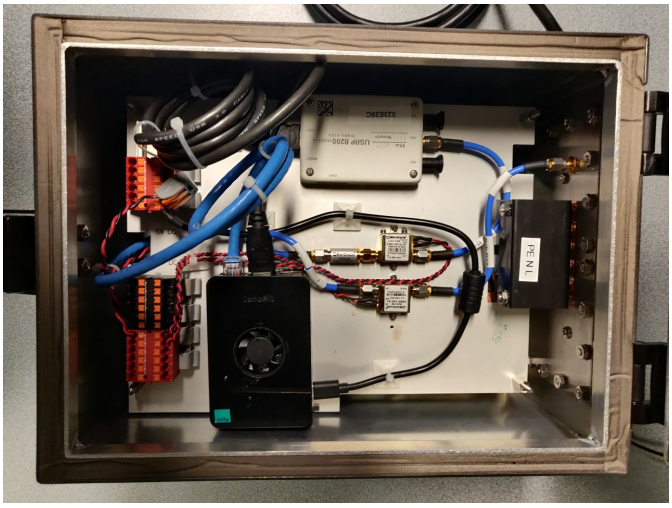

Fig. 5: **Top level of the EMI Enclosure**

Pi OS Lite version 10 (name "Buster", dated 2021-05-07). The same USB connection that powers the USRP is used to control the SDR and transfer data from the SDR to the host. Data collections on the SDRs are controlled from the host using the USRP Hardware Drivers (UHD) Python 3 API. To minimize unwanted emissions coming from the SBC, Wi-Fi and Bluetooth are permanently disabled by blacklisting the modules via rfkill and disabling wpa_supplicant as well as Bluetooth. Since this only leaves the Ethernet connection for communication, a number of additional Python libraries and Linux packages are required to make the sensor system more plug-and-play. The UHD API is complemented by msmtp, mmtp-mta, and mailutils to enable the SBC to automatically report its IP address as well as its remaining capacity, CPU usage, and temperature. This makes it possible to receive the devices IP address as long as an Internet connection is given. The rsync utility is used to automatically backup data as long as the SBC is connected to a local network and has a route to a remote server. If no connection to any remote storage location is available, rsync is used to manually offload data between data collections. Git is used to ensure version control and maintain the same codebase version on all deployed sensors. The codebase consists of a Python 3 application that accesses the UHD Python API to start the I/Q data stream and schedule the intervals I/Q in which samples are recorded on the host. The application is configured to use the external clock source provided through the WR-LEN. Data are transferred from the SDR to the host in a 16 bit signed integer format and stored in the same format to keep processing time at a minimum. Each I/Q data sample therefore requires 4 Bytes of storage.[1] A one second long sample of 20 MHz bandwidth and a matching sampling rate of 20 million (complex) samples per second for instance results in 80 million Bytes or 76.2939 MB/s. Due to the large amounts of data generated this way, the

[1]Each complex sample consists of a 16 bit in-phase and a 16 bit quadrature sample for a total of 32 bits or 4 Bytes per complex sample.

Fig. 6: **Drone Survey Overview**

Python application will be configured in the future to calculate the current environment's noise floor and only store samples above a specified threshold.

The data collection Python application can be launched using a single command-line command or using a graphical user interface (GUI) written with the Python tkinter library. Using this GUI, multiple SBCs can be controlled remotely at the same time. This also makes it possible to launch data collections on multiple sensors or schedule them to start at a common start time in the future and end together at the same time. In the interest of test configuration management, test initiation is under most circumstances controlled from this central GUI running on an on-site computer on the same subnet as the field sensors. Using the central GUI minimizes potential complications from user input error and enables computer-generated scheduling of tests based on human-readable date and time inputs. Without the GUI, tests need to be instantiated manually on multiple different remote hosts, and test delays would need to be calculated manually. This is especially important when sweeping across frequencies as a delay would cause individual sensors to record the same frequency at different times. When using the GUI's delay parameter, each SBC's Python application waits for a set delay time before initiating the survey. Once the delay is over, data collection begins on the host at the scheduled intervals and continues until the final sample has been collected.

Several steps are taken to maintain proper documentation during a RF survey. The survey Python application maintains a log file that is regularly updated as files are created, stored, moved or if a variety of errors occur. Logs are written both to syslog and local files that are rotated and synced daily via rsync. A script loaded via a cron job regularly checks the most current log files for errors and reports back to the administrator using the mailing utilities. To ensure all data can be properly identified and recovered, each file is labeled with the SBC's hostname, the SDR's serial number and a timestamp that consists of full date and time with 6 decimal points. Additionally, each file is accompanied with a JSON file recording the most important parameters, including hostname, serial number, location, latitude and longitude, center frequency, interval, length of the recording, the SDR's gain setting, sampling rate, and bit depth of the I/Q data file. Finally, if a remote storage location with rsync is used, the remote storage is manually checked for arriving I/Q data files after initiating a new survey.

C. Drone Survey

For the drone survey at HCRO, a DJI M300 [27] is used carrying a shielded box of 7.0" x 7.0" x 2.0". The shielded box houses the SDR and the data collection host. A 11 V lithium ion battery and a 5 V regulator inside the box are sufficient to power both devices. A SMA input connector is used to connect the SDR inside the box to an antenna attached to the outside of the shielded box. Proper shielding has been tested in a test chamber and with an Anritsu spectrum analyzer. The drone is rated for a maximum wind resistance of 15 m/s, a maximum payload of 930 g, and a maximum flight time of 55 minutes [27]. These capabilities are sufficient to carry the shielded box with the sensor up to the drone's regulatory maximum altitude of 400 ft.

At each location illustrated in Figure 6 and II the drone will maintain 4 different heights for 11 minutes and 40 seconds while the sensor sweeps the frequency range from 400 to 1800 MHz. While the DJI M300 promises a maximum flight time of 55 minutes, this promise can only be fulfilled under ideal conditions. The ideal flight time is reduced due to the sensor payload and environmental factors such as wind. Since a more realistic flight time is anywhere between 30 to 40 minutes, the surveys are split into two parts: 2 surveys at 400 and 300 ft, followed by recharging the drone's battery and transferring collected I/Q data from the host to a backup server, and 2

surveys at 200 and 100 ft, followed again by recharging and data transfer.

TABLE II: **Drone Locations**

ID	*Lat./Long.*	*Ground Dist. to Tx*
D1	40.8172N 121.4692W	767ft
D2	40.8160N 121.4615W	2,154ft
D3	40.8167N 121.4720W	75ft

This cycle is repeated at each location, for a total of 6 flights. Additionally, since the SDRs can cover frequencies up to 6 GHz, a further survey covering the frequencies from 1.8 to 6 GHz is added. Because the data collection host's local storage does not provide enough space to carry I/Q data for the entire 4.2 GHz sweep, the 1.8 - 6 GHz survey is again split into equal parts: a first survey covering the frequencies from 1.8 to 3.9 GHz and a second survey covering the frequencies from 3.9 to 6 GHz. These final two surveys are only conducted once at a height of 400 ft at location 1 in Figure 6.

IV. Preliminary Results

For this measurement activity, data was recorded from six spectrum sensors simultaneously: the five fixed stationary spectrum sensors located on the ground (ground sensors) and the airborne spectrum sensor that was carried by the drone (drone sensor), which was kept stationary at a fixed altitude during the various data collection periods. Two spectrum surveys were conducted with the drone sensors: survey 1 covered the frequencies from 400 to 1800 MHz at 4 different heights and survey 2 covered the frequencies from 1.8 to 6 GHz at a single height. While windy on occasion, weather conditions were fairly consistent across all surveys and well within the drone's capabilities.

A. Survey 1: 400 MHz to 1800 MHz

The six spectrum sensors (ground and drone sensors) were tasked to sweep the frequency span from 400 MHz to 1800 MHz collecting any emissions that might occur in a blind spectrum survey. The sweep recorded the 1.4 GHz range in 70 20 MHz wide steps, recording each step for 1 second and resulting in 5.2154 GB of data per sweep. In addition to the emissions existing at the site from largely unknown emitter, a test signal was purposely emitted in the form of a known ground based carrier wave (single tone) emitted at 462.6 MHz set to a power level of 0 dBm. The drone sensor's effective altitudes during the frequency sweeps were h1 = 393.4 ft, h2 = 299.9 ft, h3 = 199.8 ft, and h4 = 99.8 ft.[2] The various altitudes of the drone would act as a change in antenna height and, given the terrain, would reveal insight into the terrain's protection from emitters that may be transmitting beyond the LOS ridge lines surrounding the site.

Figure 7 shows the captures of the single tone emitted at 462.6 MHz with frequency on the x-axis and power spectral density (PSD) on the y-axis. Sensor 04, located approximately 775 ft west of the transmitter emitting the test tone, was used to verify detection of the tone on the ground. Figure 7 (a) was recorded prior to the test tone being emitted and shows no signal present at 462.6 MHz. Figure 7 (b) conversely was recorded with the test tone transmitted at 462.6 MHz and can be found just to the right of the 462.5 MHz grid line. As the PSD plots highlight, several other tones were present between 460 and 465 MHz whose origin is unknown.

With the presence of the test tone confirmed, the test moved on to evaluating altitude differences. The recorded I/Q data was condensed into 5 statistical estimates: the 5th, 25th and the 75th power percentile, as well as the median and average power. Figure 8 shows the results of recording the test tone at the 4 altitudes. As expected, the signal strength increased at location 1 as the drone's altitude decreased, decreasing the distance to the transmitter. Location 2, located 2130 ft east of the transmitter with a building and a slope blocking line of sight (LOS), shows increased signal strength as the drone increased its altitude due to improved LOS conditions and potentially unknown signals being received. Location 3, located next to sensor 04 at a distance of approximately 768 ft, demonstrated very little difference between the various heights although a slight increase in power at lower altitude thanks to being in LOS of the transmitter and its LOS distance varying at most by less than 100 ft.

Since the recordings with center frequency at 470 MHz not only confirmed receiving the test tone but furthermore a difference in signal strength at different altitudes, the testbed experiments next moved on the the frequency band recorded from 740 to 760 MHz. A number of LTE and FirstNET bands are known to be transmitted within or overlapping this frequency range. The objective therefore was to determine whether the terrain provides any protection. Two FirstNET transmitters are located south of HCRO near Old Station and one transmitter is located west of HCRO on Burney Mountain north of Freaner Peak.

Figure 9 demonstrates again that, as expected, the received power drops as the drones altitude decreases, with Location 1 next to the main office building being the sole exception. Surprisingly, the samples recorded at 300 ft show the lowest power values across various statistics while all other altitudes follow the expected order. This might indicate that, besides ground level, an altitude of approximately 300 ft is the least favorable to the path of the emitted signal.

Figures 10 (a) through (f) detail the signals recorded from 740 to 760 MHz. This 20 MHz wide band overlaps with a variety of downlink LTE and public safety bands, specifically Band 13 from 746 – 756 MHZ, Band 17 from 734 – 746 MHz, Band 12 from 729 – 746 MHz, and the FirstNET band from 758 – 763 MHz. All 6 spectrograms are clearly able to identify Band 13 at all heights from 400 to 100 ft and can even still be detected on the ground, albeit at much lower power levels. While the reduced signal strength is only easily identifiable on the spectrograms of Location 1, the PSD graphs in Figure 11 more clearly demonstrate the difference. All plots are scaled

[2]The drone's actual altitude varied due to environmental factors such as wind during Survey 1 and 2 but always stayed within a few decimal points of the reported altitude.

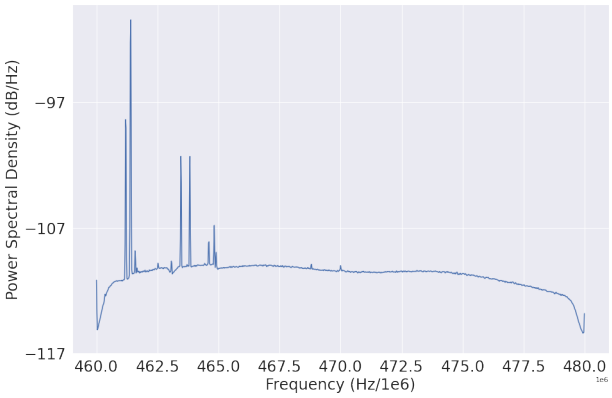

(a) Sensor 04 without the single tone present.

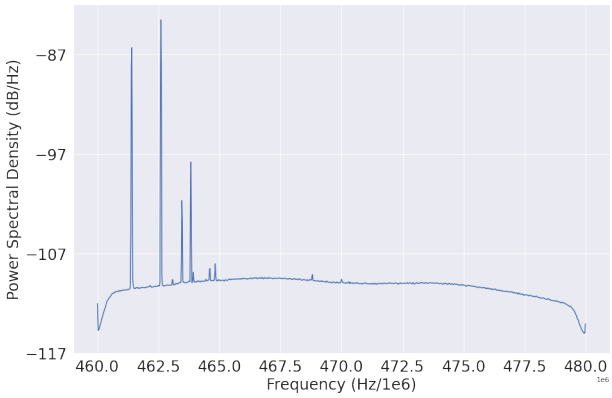

(b) Sensor 04 with the single tone present.

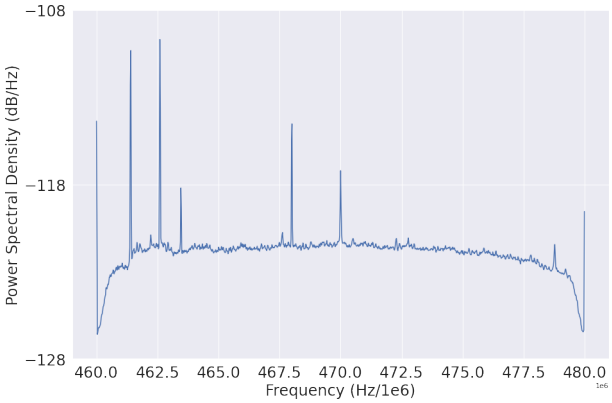

(c) Drone Sensor at 400 ft.

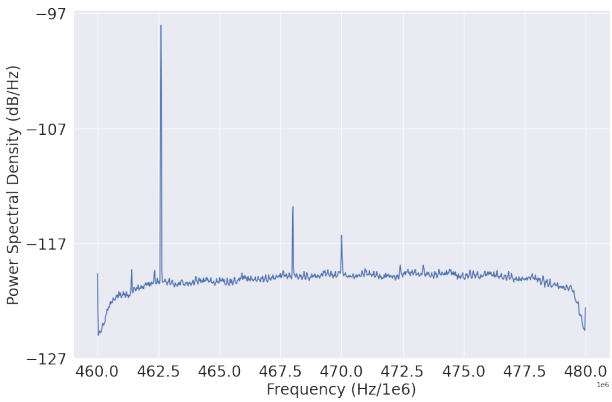

(d) Drone Sensor at 100 ft.

Fig. 7: **Power Spectral Density Plots of the I/Q data recordings centered at 470 MHz.**

to the same range, clearly indicating the drop in power when moving from 400 ft down to 100 ft, showing how the terrain helps HCRO with protecting their instruments from unknown emitters.

B. Survey 2: 1.8 GHz to 6 GHz

In this second higher frequency survey, the six spectrum sensors (ground and drone sensors) were tasked to sweep a span of 1.8 GHz to 6 GHz and collect any emissions that might occur in a blind spectrum survey. Due to the amount of time an in depth sweep takes and the limited drone battery life, the large frequency sweep was split into two parts: sweep one covered 1.8 GHz to 3.9 GHz and sweep two covered 3.9 GHz to 6 GHz. In addition to the emissions existing at the site from largely unknown emitter, two test signals were emitted purposely. A known ground based carrier wave (single tone) was emitted at 2.437 GHz and at 5.270 GHz, set to a power level of -10 dBm. Different from survey one, due to the length of sweeping the entire range and the limited drone battery life, the drone sensor was tasked to only collect a full spectrum sweep at an approximate altitude of h1 = 391.7 - 393.4 ft.

Since the drone was only flown at a single altitude for Survey 2, the spectrogram of the I/Q data recording is this time compared to the ground sensors. Remember that the sensor carried by the drone is sensor 06. Figure 12 shows the samples recorded simultaneously at the 6 different locations depicted in Figure 1. While the drone sensor (Figure 12 (f)) depicts the Band 2 LTE downlink signals most clearly, Sensor 01 on top of the main office's building at a height of close to 30 ft still receives a fairly clear signal. Sensor 02 is most likely protected by tree cover and does not see the same emissions, neither do Sensors 02 and 05. Surprisingly, Sensor 04 is still able to detect the LTE signal, albeit at a noticeably lower strength.

Finally, a frequency band overlapping with a known satellite signal was analyzed. 2320 - 2345 MHz is a shared band allocated to satellite communication in the United States. It is shared between satellite communication, aeronautical telemetry, mobile, radiolocation, and point to point data links among others [28]. Most of the bands within this 25 MHz range are used by a variety of Sirius XM Radio satellites. Figure 14 shows footprints of multiple satellite radio signals on a spectrogram from data recorded by Sensor 04. Figure 13 compares the PSD of the data recorded by all 6 sensors. Sensor 01 receives the strongest signal due to its higher gain antenna, followed by Sensor 04. Sensor 02, located in an area

htbp]

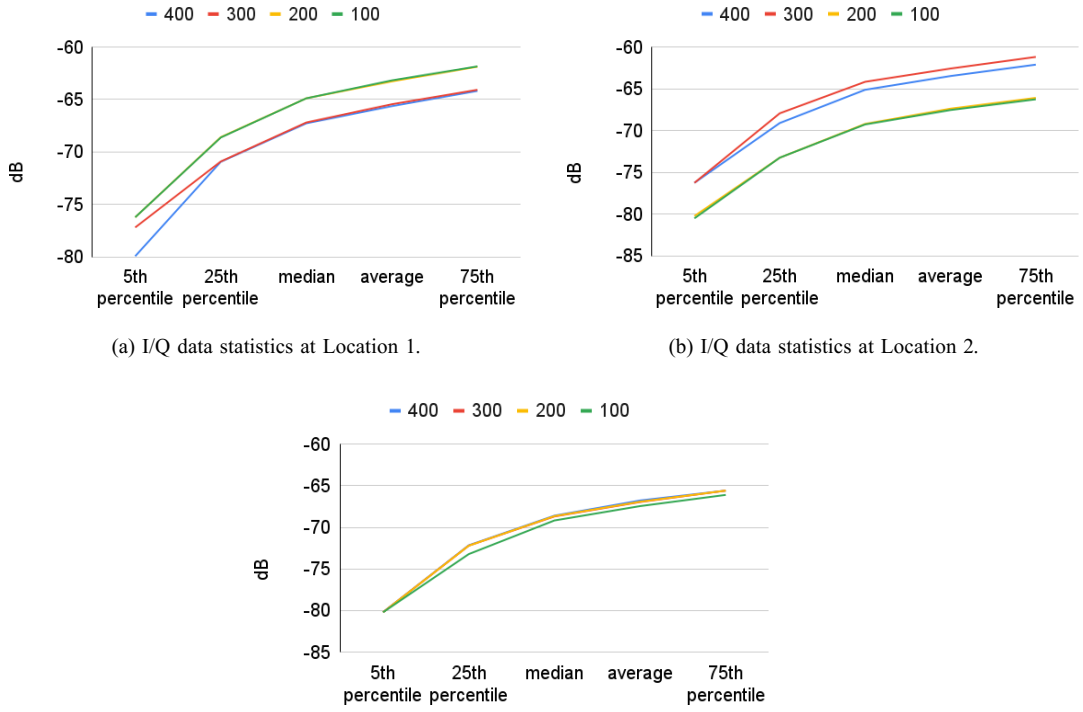

(a) I/Q data statistics at Location 1.

(b) I/Q data statistics at Location 2.

(c) I/Q data statistics at Location 3.

Fig. 8: **I/Q data converted to various signal statistics for the data recorded with center frequency at 470 MHz.**

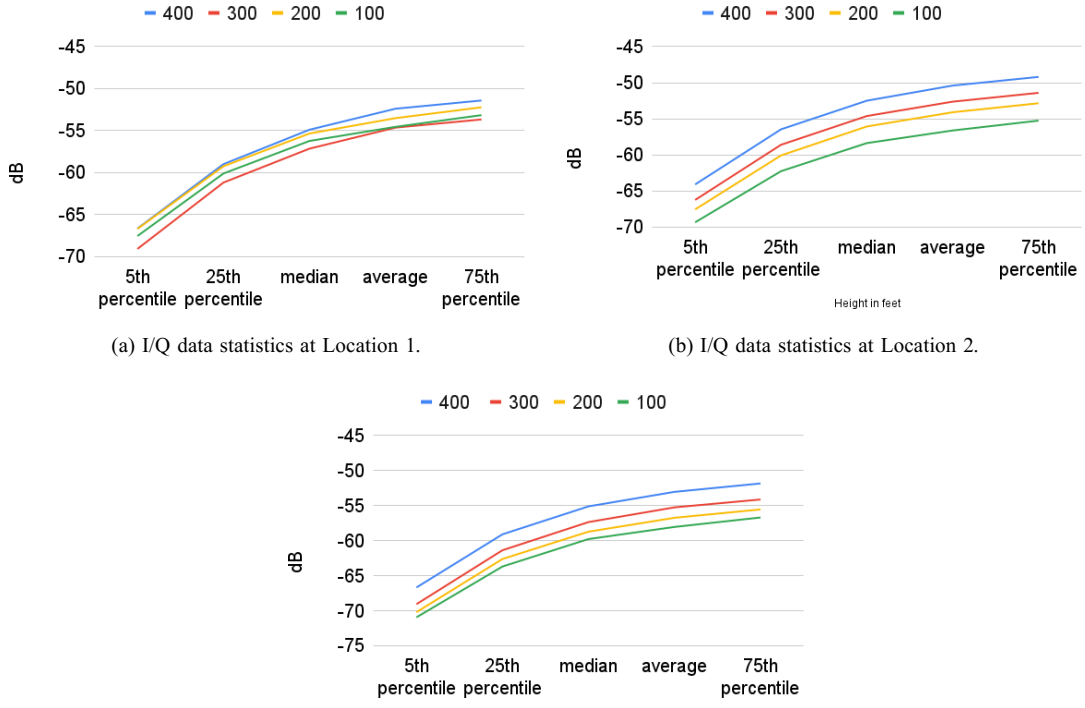

(a) I/Q data statistics at Location 1.

(b) I/Q data statistics at Location 2.

(c) I/Q data statistics at Location 3.

Fig. 9: **I/Q data converted to various signal statistics for the data recorded with center frequency at 750 MHz.**

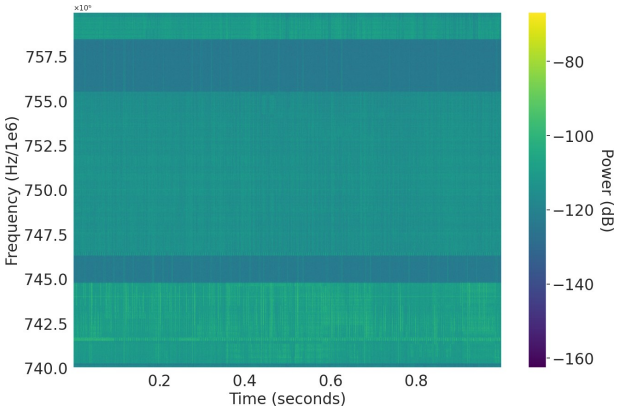

(a) Drone Sensor at location 1 at 400 ft.

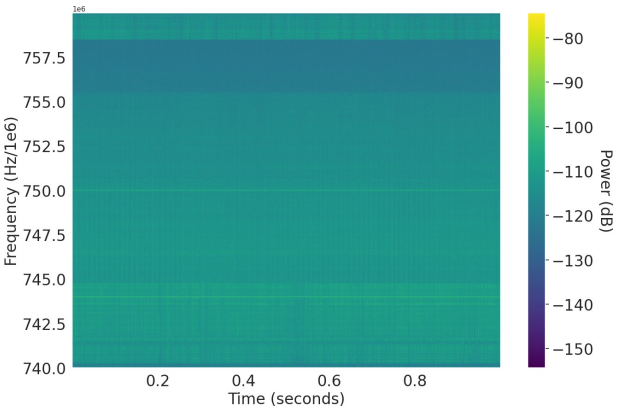

(b) Drone Sensor at location 1 at 100 ft.

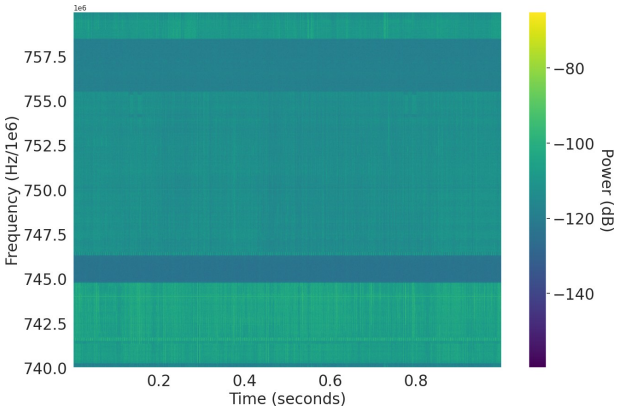

(c) Drone Sensor at location 2 at 400 ft.

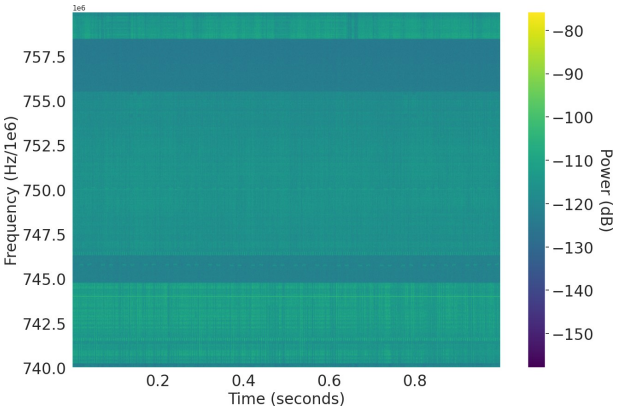

(d) Drone Sensor at location 2 at 100 ft.

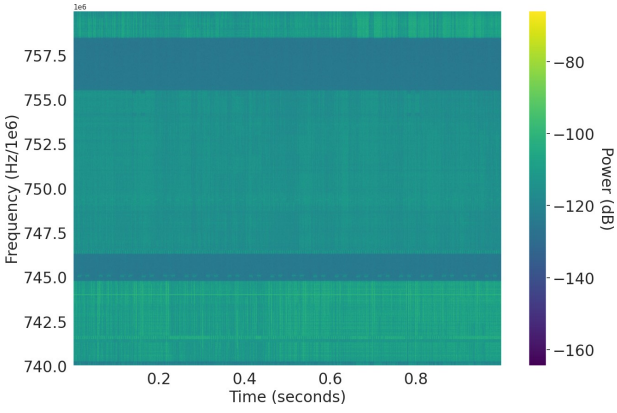

(e) Drone Sensor at location 3 at 400 ft.

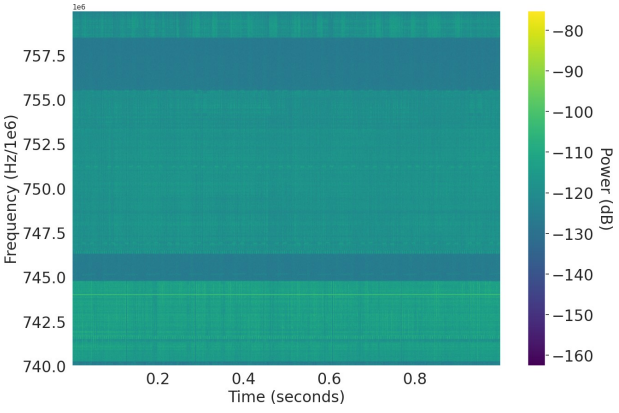

(f) Drone Sensor at location 3 at 100 ft.

Fig. 10: **Spectrograms of the I/Q data recordings centered at 750 MHz.**

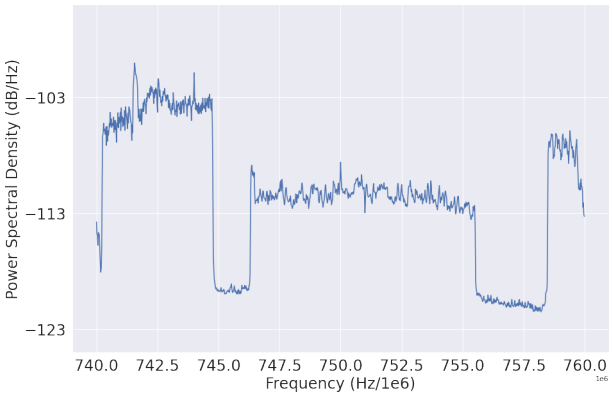

(a) Drone Sensor at location 1 at 400 ft.

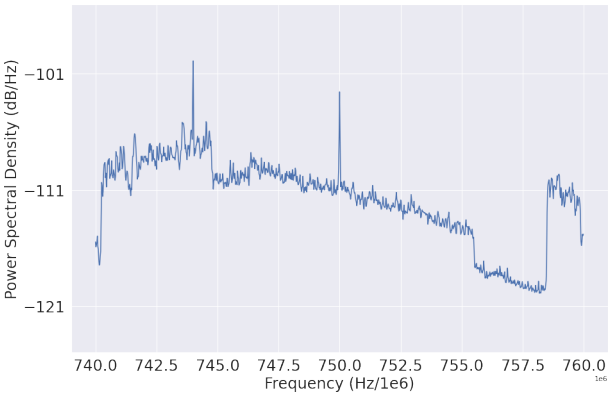

(b) Drone Sensor at location 1 at 100 ft.

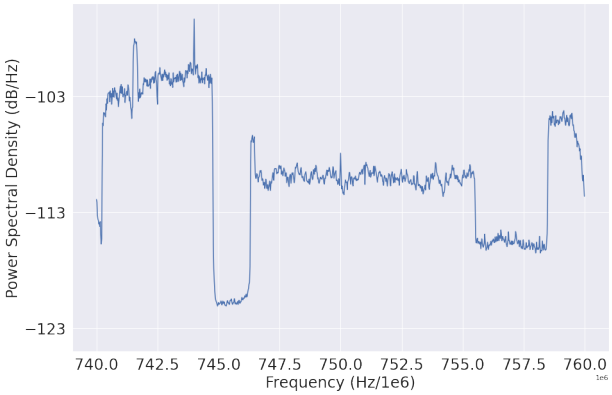

(c) Drone Sensor at location 2 at 400 ft.

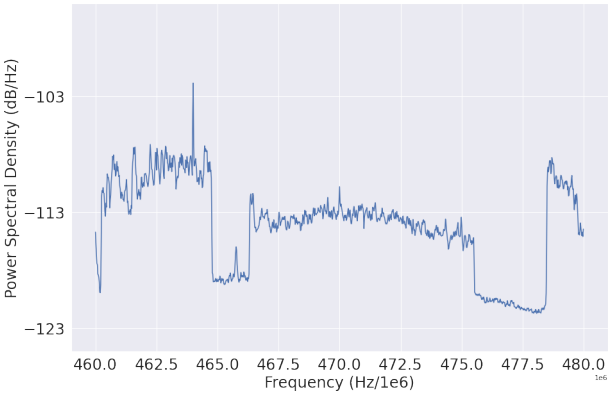

(d) Drone Sensor at location 2 at 100 ft.

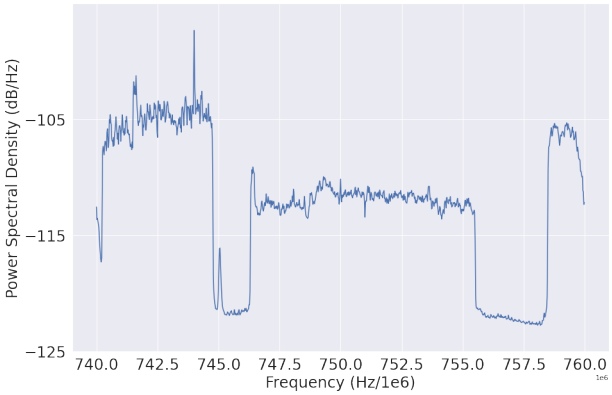

(e) Drone Sensor at location 3 at 400 ft.

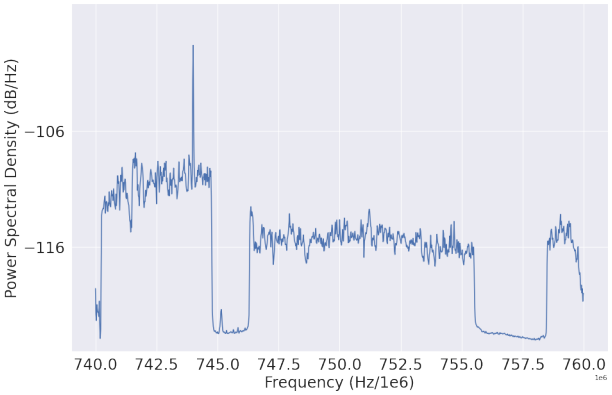

(f) Drone Sensor at location 3 at 100 ft.

Fig. 11: **Power Spectral Density Plots of the I/Q data recordings centered at 750 MHz.**

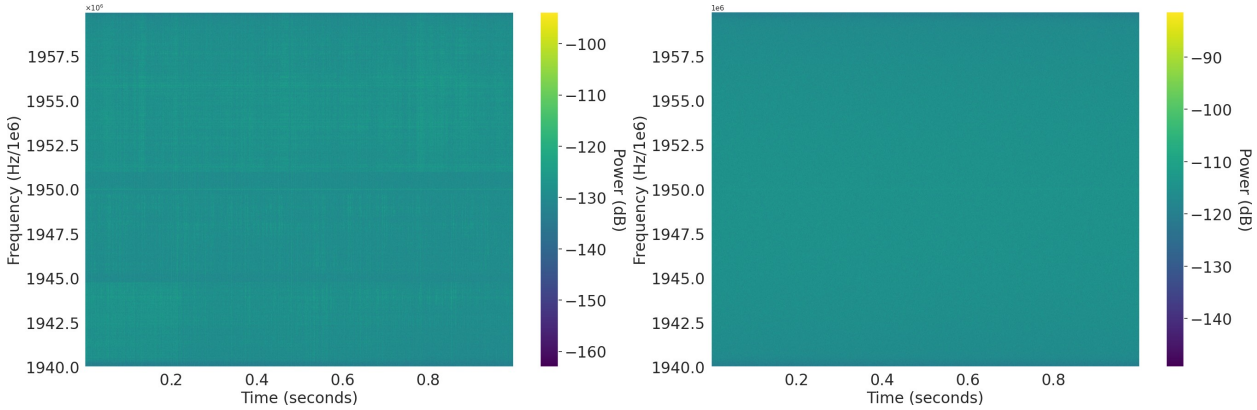

(a) Sensor 01 recording at 1950 MHz.

(b) Sensor 02 recording at 1950 MHz.

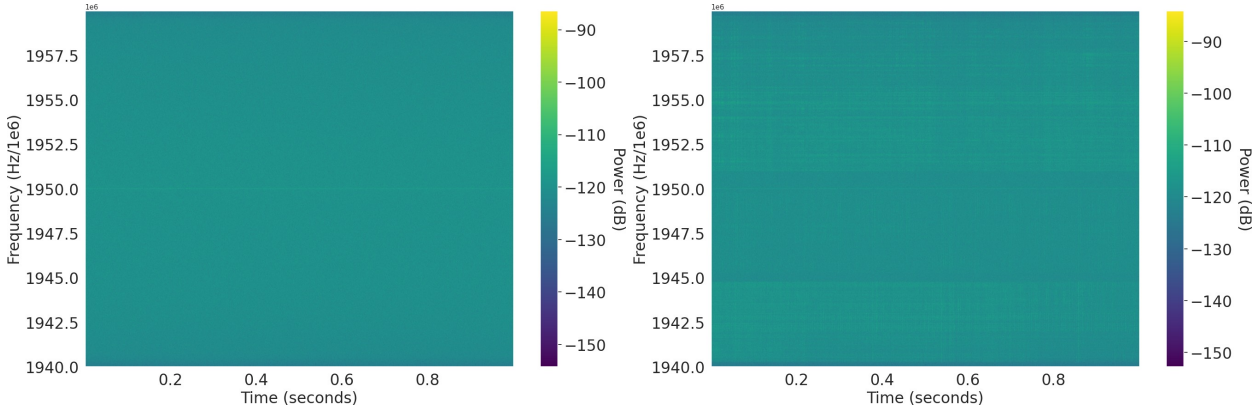

(c) Sensor 03 recording at 1950 MHz.

(d) Sensor 04 recording at 1950 MHz.

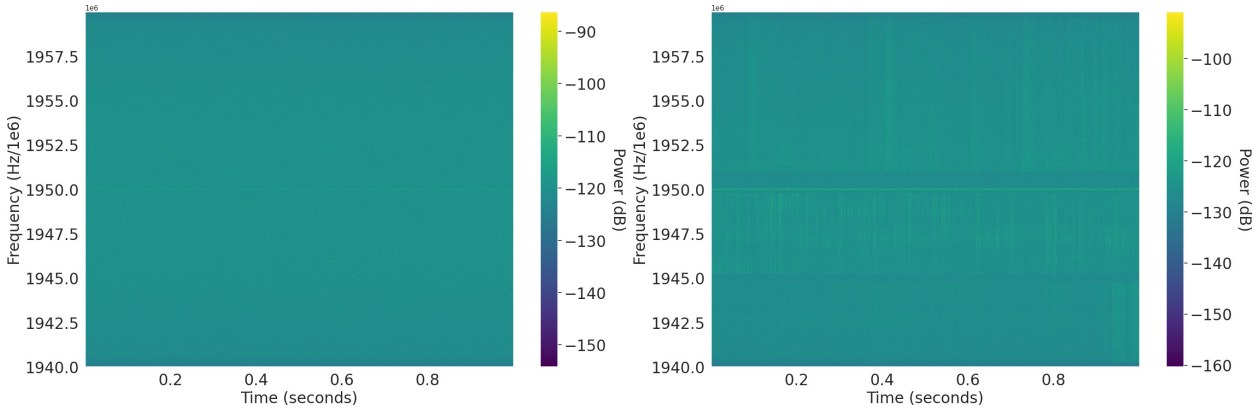

(e) Sensor 05 recording at 1950 MHz.

(f) Sensor 06 recording at 1950 MHz.

Fig. 12: **Spectrograms of the I/Q data recordings centered at 1950 MHz.**

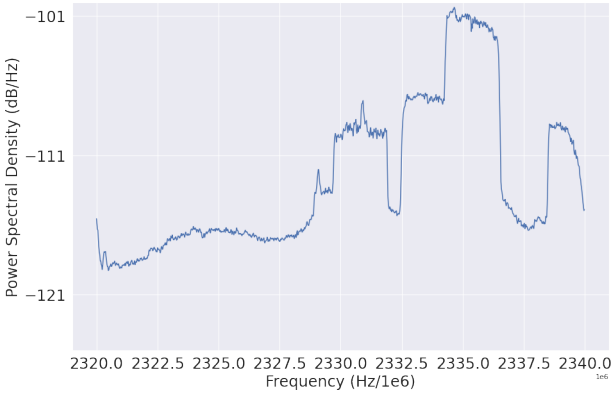

(a) Sensor 01 recording at 2330 MHz.

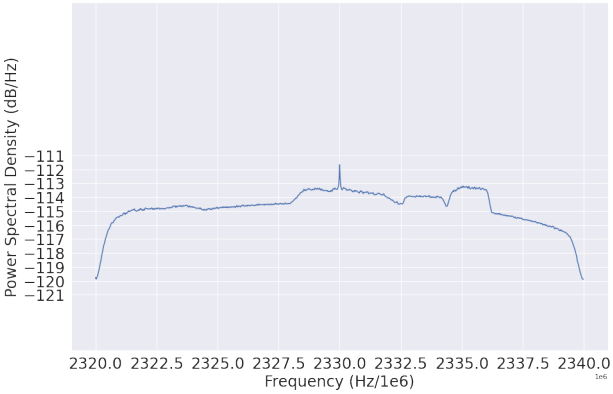

(b) Sensor 02 recording at 2330 MHz.

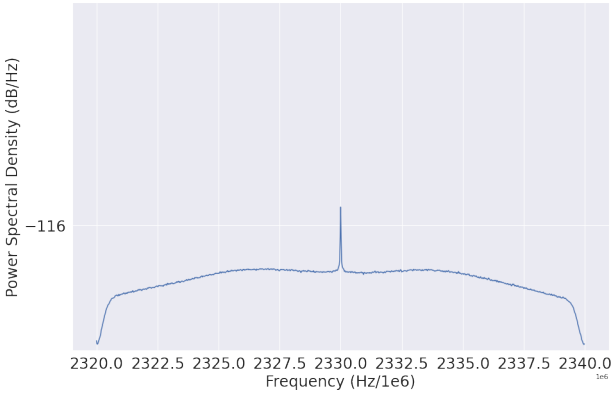

(c) Sensor 03 recording at 2330 MHz.

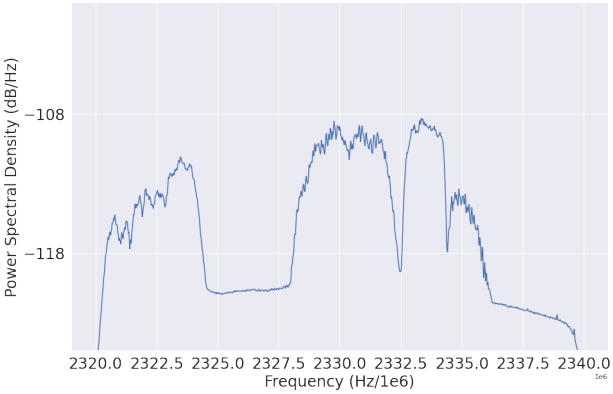

(d) Sensor 04 recording at 2330 MHz.

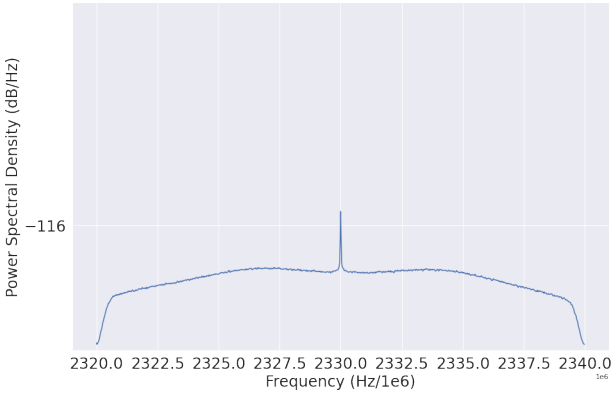

(e) Sensor 05 recording at 2330 MHz.

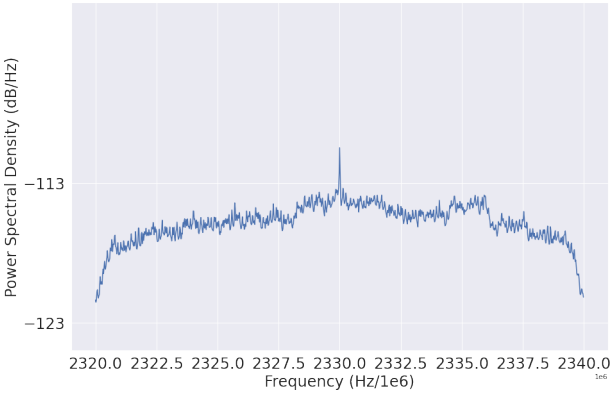

(f) Sensor 06 recording at 2330 MHz.

Fig. 13: **Spectrograms of the I/Q data recordings centered at 1950 MHz.**

with substantial tree cover only faintly detects the same signal, as does Sensor 06 at 400ft carried by the drone.

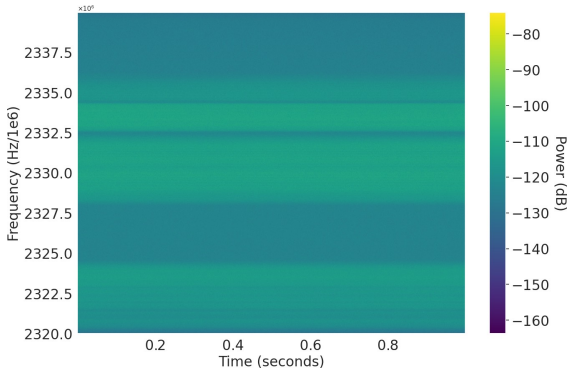

Fig. 14: **Sirius XM Signal at 2330 MHz recorded by Sensor 04.**

A number of issues were uncovered during this test. Due to video being transmitted from the drone to its controller using the 2.4 GHz unlicensed band at 29.5 dBm [27], recordings of any band within that range or even nearby bands, such as the satellite communications band, was saturated by the strong signal transmitted from the drone. Without the video transmission, the satellite radio signal would be much clearer on the drone sensor. Additionally, while first suspected of being a feature of the various locations, Sensors 03 and 05 seem to suffer from a disconnected antenna or a similar issue preventing the SDR from detecting any signals. The same behavior observed in the 1950 MHz and the 2330 MHz bands, was also observed in the bands carrying the test signals.

V. Conclusion

In summary, the testbed's first results show how relatively low-cost SDRs can be used to measure RFI at a radio astronomy facility. Ettus USRP B200 mini SDRs were used to detect a variety of emissions at the facility, including a number of unknown tones around 462 MHz, FirstNET and LTE bands 2/12/13/17 in the 740 - 760 MHz and 1940 - 1960 MHz ranges, as well as satellite signals in the 2320 - 2340 MHz band. While none of these bands directly overlap with frequencies allocated to radio astronomy, they show the potential danger of locating powerful signal sources near radio astronomy, both in frequency and in space. These first 2 surveys provide important results how radio astronomy could be protected in a shared spectrum environment, highlighting that the facility's location is as important as sharing in time and frequency can be.

As the testbed continues to grow and expand its scope, a number of sensor improvements and potential failures are uncovered. Sensor 01 is suspected to be located too close to other transmitters or an unintentional radiator that saturates the SDR's ADC at certain frequency ranges. Similar behavior can be observed in Sensor 02 data, where the noise floor is consistently raised compared to other sensors (see Figure 13 and compare (b) with (c) and (e)). Finally, Sensors 03 and 05 need to be investigated for loose connectors or a similar issue.

Still, despite a few minor complications, establishing a testbed at the Hat Creek Radio Observatory and analyzing to what degree the observatory's environment provides protection from RFI was an important first step towards creating a spectrum sharing environment conducive to radio astronomy. In a next step, the single test tone used for verification can be replaced by an actual signal to measure different types of RFI. Furthermore, while initial sensor issues are ironed out, the testbed will next focus on establishing radio astronomy observation windows that are free from satellite interference by creating a database of satellites whose beam overlaps with the radio observatory instead of a database with all satellites passing overhead.

Acknowledgment

The authors would like to thank the HCRO team for their ongoing collaboration and support and Thomas Brinkoetter from Radio Site Test for supporting the RF surveys with his drone and expertise.

References

[1] C. Barnbaum and R. F. Bradley, "A new approach to interference excision in radio astronomy: Real-time adaptive cancellation," *The Astronomical Journal*, vol. 116, no. 5, pp. 2598–2614, nov 1998. [Online]. Available: https://doi.org/10.1086/300604

[2] I. Sihlangu, N. Oozeer, and B. A. Bassett, "Multi-dimensional radio frequency interference framework for characterizing radio astronomy observatories," *Journal of Astronomical Telescopes, Instruments, and Systems*, vol. 8, no. 01, oct 2021. [Online]. Available: https://doi.org/10.1117%2F1.jatis.8.1.011003

[3] C. Wilson, "Propagation prediction in establishing a radio quiet zone for radioastronomy," in *The 8th European Conference on Antennas and Propagation (EuCAP 2014)*, 2014, pp. 1209–1213.

[4] Wireless Innovation Forum. Passive and active spectrum sharing focus of new wireless innovation forum project. Online; accessed 21-September-2022. [Online]. Available: https://www.prnewswire.com/news-releases/passive-and-active-spectrum-sharing-focus-of-new-wireless-innovation-forum-project-301342415.html

[5] National Radio Astronomy Observatory. (2022) The history of radio astronomy. Online; accessed 09-September-2022. [Online]. Available: https://public.nrao.edu/radio-astronomy/the-history-of-radio-astronomy/

[6] T. E. Gergely, "Spectrum access for the passive services: The past and the future," *Proceedings of the IEEE*, vol. 102, no. 3, pp. 393–398, 2014.

[7] D. R. DeBoer, S. L. Cruz-Pol, M. M. Davis, T. Gaier, P. Feldman, J. Judge, K. I. Kellermann, D. G. Long, L. Magnani, D. S. McKague, T. J. Pearson, A. E. E. Rogers, S. C. Reising, G. Taylor, A. R. Thompson, and L. van Zee, "Radio frequencies: Policy and management," *IEEE Transactions on Geoscience and Remote Sensing*, vol. 51, no. 10, pp. 4918–4927, 2013.

[8] V. Pankonin and R. Price, "Radio astronomy and spectrum management: The impact of warc-79," *IEEE Transactions on Communications*, vol. 29, no. 8, pp. 1228–1237, 1981.

[9] C. Crockett. How radio astronomy put new eyes on the cosmos. ScienceNews. Online; accessed 09-September-2022. [Online]. Available: https://www.sciencenews.org/article/radio-astronomy-history-cosmos-black-hole-planet-universe

[10] R. Umar, Z. Z. Abidin, Z. A. Ibrahim, M. S. R. Hassan, Z. Rosli, and Z. S. Hamidi, "Population density effect on radio frequencies interference (rfi) in radio astronomy," *AIP Conference Proceedings*, vol. 1454, no. 1, pp. 39–42, 2012. [Online]. Available: https://aip.scitation.org/doi/abs/10.1063/1.4730683

[11] G. Hellbourg and I. Morrison, "Cyclic imaging for all-sky interference forecasting with array radio telescopes," in *2019 RFI Workshop - Coexisting with Radio Frequency Interference (RFI)*, 2019, pp. 1–5.

[12] W. van Driel, "Radio quiet, please! – protecting radio astronomy from interference," *Proceedings of the International Astronomical Union*, vol. 5, no. S260, p. 457–464, 2009.

[13] C. Beaudet, J. Ford, T. Minter, M. McCarty, K. O'Neil, and R. Prestage, "Radio frequency interference management efforts at the national radio astronomy observatory green bank site," in *2013 US National Committee of URSI National Radio Science Meeting (USNC-URSI NRSM)*, 2013, pp. 1–1.

[14] International Telecommunication Union, "Recommendation itu-r ra.769-2 - protection criteria used for radio astronomical measurements," 2004, online; accessed 09-September-2022. [Online]. Available: https://www.itu.int/dms _pubrec/itu-r/rec/ra/R-REC-RA.769-2-200305-I!!PDF-E.pdf

[15] P. Ayodele and F. Olabisi, "Interference protection of radio astronomy services using cognitive radio spectrum sharing models," in *2015 European Conference on Networks and Communications (EuCNC)*, 2015, pp. 86–90.

[16] International Telecommunication Union, "Recommendation itu-r ra.1513 - levels of data loss to radio astronomy observations and percentage-of-time criteria resulting from degradation by interference for frequency bands allocated to the radio astronomy service on a primary basis," 2015, online; accessed 09-September-2022. [Online]. Available: https://www.itu.int/dms pubrec/itu-r/rec/ra/R-REC-RA.1513- 2-201503-I!!PDF-E.pdf

[17] National Research Council, *Spectrum Management for Science in the 21st Century*. Washington, DC: The National Academies Press, 2010. [Online]. Available: https://nap.nationalacademies.org/catalog/12800/spectrum-management-for-science-in-the-21st-century

[18] P. Bolli, F. Gaudiomonte, R. Ambrosini, C. Bortolotti, M. Roma, C. Barberi, and F. Piccoli, "The mobile laboratory for radio-frequency interference monitoring at the sardinia radio telescope," *IEEE Antennas and Propagation Magazine*, vol. 55, no. 5, pp. 19–24, 2013.

[19] Cisco. Cisco annual internet report (2018–2023) white paper. Online; accessed 09-January-2022. [Online]. Available: https://www.cisco.com/c/en/us/solutions/collateral/executive-perspectives/annual-internet-report/white-paper-c11-741490.html

[20] M. J. Bentum, A. J. Boonstra, and W. A. Baan, "Impact of cognitive radio on radio astronomy," in *RFI mitigation workshop, Groningen, the Netherlands*, 2010, online; accessed 09-September-2022. [Online]. Available: https://ris.utwente.nl/ws/portalfiles/portal/5504059/CognitiveRadio V8.pdf

[21] M. J. Bentum, A.-J. Boonstra, and W. A. Baan, "The coexistence of cognitive radio and radio astronomy," 2009.

[22] Z. Z. Abidin, Z. A. Ibrahim, Z. Rosli, S. R. Hassan, S. F. F. Malim, N. Noorazlan, M. A. A. Aziz, and A. S. M. Suhaimi, "Methods and applications of radio frequency interference surveys for radio astronomy in malaysia," in *Proceeding of the 2011 IEEE International Conference on Space Science and Communication (IconSpace)*, 2011, pp. 178–181.

[23] T. Nhlapo, R. Geschke, and P. Wiid, "Emi risk assessment methodology for farming communities close to a radio quiet zone," in *2018 IEEE 4th Global Electromagnetic Compatibility Conference (GEMCCON)*, 2018, pp. 1–5.

[24] P. P. Sitompul, T. Manik, M. Batubara, and B. Suhandi, "Radio frequency interference measurements for a radio astronomy observatory site in indonesia," *Aerospace*, vol. 8, no. 2, 2021. [Online]. Available: https://www.mdpi.com/2226-4310/8/2/51

[25] I. Ku¨c¸u¨k, I. U¨ ler, and S. O¨ z, "Site selection for a radio astronomy observatory in turkey: atmospherical, meteorological, and radio frequency analyses," *Exp Astron*, vol. 33, pp. 1–26, 2012.

[26] P. A. Raybole, S. Sureshkumar, S. Katore, and S. Rai, "Real time prediction, detection and co-existing with satellite interference at gmrt," in *2016 Radio Frequency Interference (RFI)*, 2016, pp. 96–99.

[27] Da-Jiang Innovations. Matrice 300 rtk specs. Online; accessed 09-September-2022. [Online]. Available: https://www.dji.com/matrice-300/specs

[28] Federal Communications Commission. Fcc online table of frequency allocations. 47 C.F.R. § 2.106; Online; accessed 09-September-2022. [Online]. Available: https://transition.fcc.gov/oet/spectrum/table/fcctable.pdf